Lawrence Berkeley National Laboratory
LBL Publications

Title
Liberation of ion implanted Ge nanocrystals from a silicon dioxide matrix via hydrofluoric acid vapor etching

Permalink
https://escholarship.org/uc/item/8jc9w78k

Authors
Sharp, I.D.
Xu, Q.
Liao, C.Y.
et al.

Publication Date
2003

eScholarship.org Powered by the California Digital Library
University of California

Liberation of Ion Implanted Ge Nanocrystals from a Silicon Dioxide Matrix via Hydrofluoric Acid Vapor Etching

I.D. Sharp[a,b], Q. Xu[a,b], C. Y. Liao[a,b], J.W. Ager III[a], J.W. Beeman[a], K.M. Yu[a], D. Zakharov[a], Z. Liliental-Weber[a], E.E. Haller[a,b]
[a]Materials Sciences Division, Lawrence Berkeley National Laboratory, Berkeley, CA 94720
[b]Department of Materials Science and Engineering, University of California, Berkeley, CA 94720

ABSTRACT

A method to liberate germanium (Ge) nanocrystals from silicon dioxide (SiO_2) thin films by hydrofluoric acid (HF) vapor etching is presented. Multi-energy implantation of mass separated Ge ions into 500-nm-thick wet oxide layers on silicon (Si) substrates followed by thermal annealing produces nanocrystals that are 2 to 8 nm in diameter. Raman spectra exhibit the expected asymmetric line shapes due to the phonon confinement effect, but with a higher peak frequency than predicted. To free the nanocrystals, samples are etched in HF vapor to selectively remove the SiO_2 matrix and expose the nanocrystal surfaces. Raman spectra of etched samples display peak frequencies consistent with relief of compressive stress. The liberated nanocrystals show long-term stability under ambient atmospheric conditions. Ge nanocrystals can be removed from etched surfaces using an ultrasonic methanol cleaning procedure. The nanocrystal-containing solution is applied to a TEM grid and the solvent is evaporated. Subsequently obtained electron diffraction patterns confirm that the nanocrystals survive this transfer step. Thus, liberated Ge nanocrystals are expected to be accessible for a wide range of manipulation processes and direct characterization techniques.

INTRODUCTION

Ge nanocrystals have been widely investigated due to their potential optoelectronic and non-volatile memory applications [1,2], as well as their value in exploring the basic physical properties of nanocrystalline materials [3]. A variety of techniques, including ion implantation [4,5], rf co-sputtering [6,7], and inverse micelle liquid chemistry [8] have been used to prepare Ge nanocrystals. In particular, fabrication via implantation of energetic Ge ions into SiO_2 has attracted considerable interest due to its compatibility with existing microfabrication processes. Ion implantation also permits fabrication of isotopically controlled Ge nanocrystals that may be used for spintronics investigations of ^{73}Ge, selective doping of nanocrystals via neutron transmutation doping (NTD), and precise analysis of nanocrystal stress states.

Since Ge nanocrystals formed by means of ion implantation are embedded in a solid (often SiO_2) matrix, only certain optical and x-ray techniques are available for nondestructive characterization. Direct access to the nanocrystal surfaces, which would allow for contact formation and manipulation to construct 2-D arrays, relies on processes to *liberate* nanocrystals. The aim of this study is to develop a process to liberate Ge nanocrystals from SiO_2 films and transfer them between surfaces in order to expand the range of available characterization and manipulation techniques.

EXPERIMENTAL DETAILS

Silicon dioxide thin films were grown to a thickness of 500 nm by wet oxidation of (100) oriented Si substrates. Isotopically pure nanocrystals were fabricated via selective implantation of either ^{70}Ge or ^{74}Ge ions. Multi-energy implantations were performed at 50 keV (1×10^{16} cm^{-2}), 80 keV (1.2×10^{16} cm^{-2}), and 120 keV (2×10^{16} cm^{-2}) [4]. Following implantation, samples were annealed in an Ar atmosphere for various times between 30 min and 60 min and temperatures between 850 ºC and 900 ºC, and were subsequently quenched from the annealing temperature to room temperature under running water. Raman spectroscopy was used to detect the near-zone-center optical mode of confined phonons, confirming the existence of monoisotopic Ge nanocrystals. The atomic distribution of Ge was measured by Rutherford backscattering spectrometry (RBS). To obtain structural information, as well as size and spatial distributions, high-resolution transmission electron microscopy (HRTEM) was performed.

Nanocrystals were liberated from the matrix via selective hydrofluoric acid (HF) vapor etching of the oxide film using vapor from a 2:1 49% HF:H_2O solution. To remove the H_2O reaction product and ensure effective HF mass transport, the sample surface was purged with nitrogen at ten-second intervals throughout the etching process. After etching, RBS, Raman spectroscopy, and x-ray photoelectron spectroscopy (XPS) were performed to verify that the nanocrystals survived the etching process and remained on the surface.

Etched samples were sonicated in methanol for one hour to remove the liberated Ge nanocrystals. Nanocrystals were transferred to other surfaces by immersing them in the nanocrystal-containing solutions and evaporating away the methanol under constant nitrogen flow. Electron diffraction patterns were obtained to verify successful transfer of the nanocrystals.

RESULTS

Raman spectroscopy of annealed samples confirms successful fabrication of both ^{70}Ge and ^{74}Ge nanocrystals. Direct comparison of nanocrystalline Ge and bulk Ge is achieved using highly enriched ^{70}Ge and ^{74}Ge bulk single crystals [9]. Nanocrystalline Ge spectra exhibit asymmetric peak broadening and higher frequency Raman shifts compared to their bulk counterparts.

TEM images reveal an approximately 70 nm wide layer of nanocrystals in the near surface region of the oxide film, as shown in Fig. 1(a). No nanocrystals are observed in the top 50 nm of the samples. HR-TEM images show spherical nanocrystals, with and without twinning planes, with sharp interfaces between the crystals and the matrix, as shown in Fig. 1(b).

RBS profiles of samples before and after etching of the SiO_2 matrix indicate that after complete removal of the oxide film, 74% of the implanted Ge remains on the surface of the sample. Etched samples consistently exhibit lower frequency Raman peaks than the corresponding as-grown nanocrystals, as shown in Fig. 2. Raman spectra obtained just after etching also exhibit extended tails to lower energies. After five months of exposure to ambient atmospheric conditions, these low-energy tails diminish and no additional broadening of the main Raman line is observed. Preliminary XPS measurements indicate the presence of both elemental and oxidized Ge after etching and exposure.

RBS spectra prove that the ultrasonic cleaning process is successful in removing 95% of the Ge that remains on the surfaces after etching. Electron diffraction patterns, showing

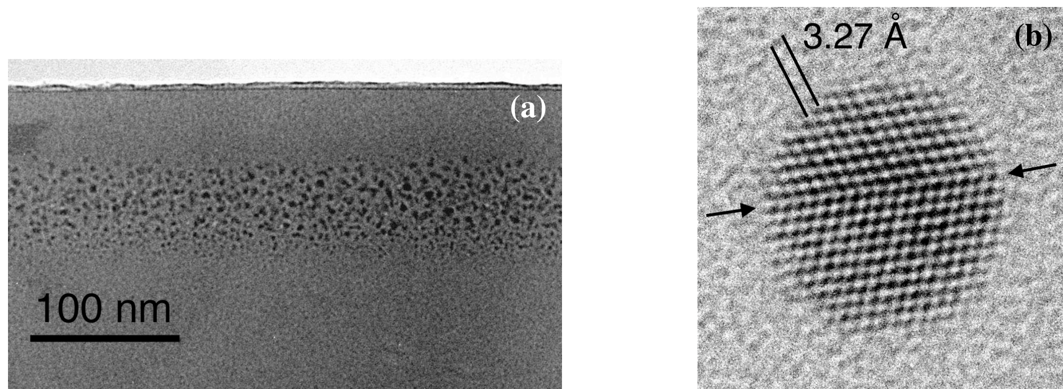

Fig. 1: (a) Cross-sectional TEM micrograph showing a band of Ge nanocrystals, 2 nm to 8 nm in diameter, in the near-surface region of the SiO_2 matrix. No nanocrystals are observed in the top 50 nm of the oxide. (b) HR-TEM micrograph of a single 5.3 nm diameter Ge nanocrystal, with arrows indicating the location of a single twinning plane.

characteristic Ge powder rings, confirm that transfer of nanocrystals between surfaces is achieved by evaporation of the methanol solvent.

DISCUSSION

Cross-sectional TEM images reveal a mean nanocrystal diameter of 5 nm, with a distribution between 2 nm and 8 nm. Although Ge concentrations in the near surface region should be sufficient to produce nanocrystals, none are observed in the top 50 nm of the implanted and annealed samples. Furthermore, the size distribution varies with depth. The band initiates sharply with large nanocrystals and the sizes smoothly decrease with depth. Similar observations were previously reported by Heinig *et al.* [10,11], who convincingly concluded that the oxidation of dissolved Ge via in-diffusion of oxygen suppresses nanocrystal formation near the surface.

Comparison of Raman spectra from as-grown samples and isotopically enriched bulk single crystals confirms the existence of monoisotopic Ge nanocrystals. As expected, ^{70}Ge bulk crystals and nanocrystals exhibit higher energy Raman line shifts than their ^{74}Ge counterparts. Raman spectra of nanocrystals in SiO_2, shown in Fig. 2(b), demonstrate asymmetric peak broadening consistent with the phonon confinement model proposed by Richter *et al.* [12]. Phonon confinement theory predicts the Raman peak from nanocrystals to be redshifted in relation to the bulk spectrum. Raman spectra of as-grown nanocrystal samples, however, consistently display peaks at higher energies than the corresponding bulk crystals, while liberated nanocrystals exhibit the theoretically expected redshift [Fig. 2]. As a result of rapid quenching from the annealing temperature the SiO_2 does not relax the strain developed during the growth phase of the nanocrystals, resulting in the observed blueshift [13]. Subsequent removal of the matrix via HF vapor etching necessarily removes the source of strain and returns the nanocrystals to a relaxed state. Results from ongoing x-ray diffraction experiments will allow more complete characterization of the stress states of the as-grown and liberated nanocrystals.

The Raman spectrum shown in Fig. 2(c), obtained two hours after etching, shows an extended tail to lower energies which is not observed in as-grown samples [Fig. 2(b)]. This broadening is characteristic of high amplitude, low energy surface phonon modes [6]. In as-

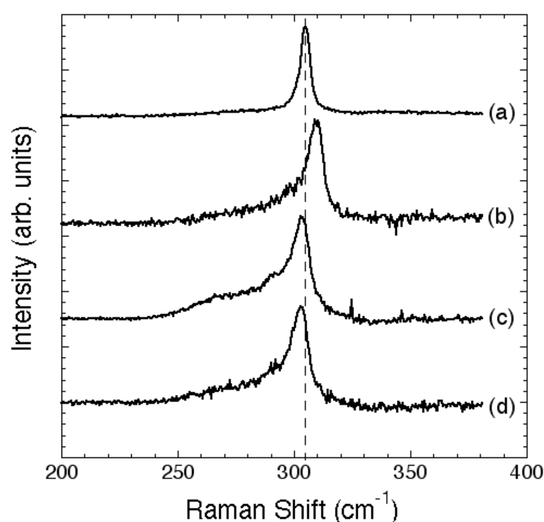

Fig. 2: Raman spectra of isotopically pure bulk ^{70}Ge (a), as-grown nanocrystals (b), liberated nanocrystals after two hours exposure to air (c), and liberated nanocrystals after five months exposure to air (d). The dashed vertical line shows the location of the bulk Ge reference peak. The blue shift seen in (b) is attributed to hydrostatic pressure that is relieved with etching.

grown nanocrystals, these modes are suppressed due to interface interactions with the matrix. Immediately after etching, however, nanocrystals are hydrogen terminated, and the surface atoms are less tightly bound than interior atoms, though it is unlikely such passivation would be effective over extended times. After prolonged exposure to ambient atmospheric conditions the broad tail fades [Fig. 2(d)], which suggests surface GeO_2 formation suppresses lower energy phonon modes. Although Raman spectra do not directly reveal the presence of GeO_2, possibly due to the detection limit, preliminary XPS measurements of liberated and exposed nanocrystals do indicate the presence of both oxidized and elemental Ge. Results of ongoing experiments should provide a more complete understanding of the mechanism and effects of oxide formation. For nanocrystals to remain stable over time, as observed experimentally, the native oxide of nanocrystalline Ge may either be self-limiting after oxidation of just a few monolayers or the kinetics of oxide formation may be greatly suppressed in the nanocrystalline form.

The full width at half maximum (FWHM) of both the as-grown nanocrystals and the liberated nanocrystals after five months of exposure is 8 cm^{-1}, indicating that the broadening observed immediately after etching (FWHM = 12 cm^{-1}) is the result of low energy surface

Fig. 3: Ge distribution measured by RBS showing Ge concentration profiles for as-grown nanocrystals in 500 nm SiO_2 (o), and after etching of 140 nm SiO_2 (♦), 240 nm SiO_2 (▲), and 410 nm SiO_2 (■). The vertical dashed line represents the Si/SiO_2 interface for all spectra. After etching, 74% of the total implanted Ge accumulates on the surface.

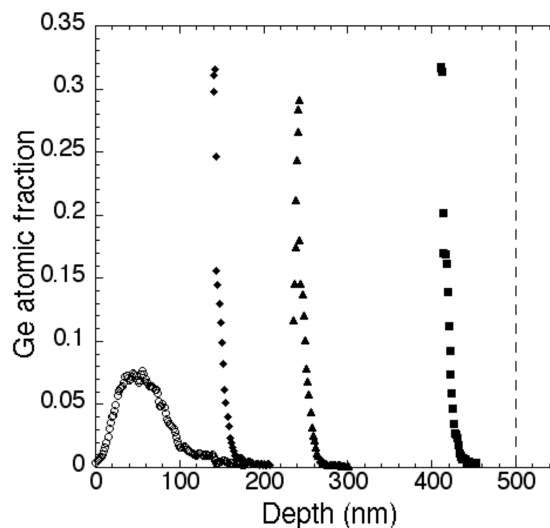

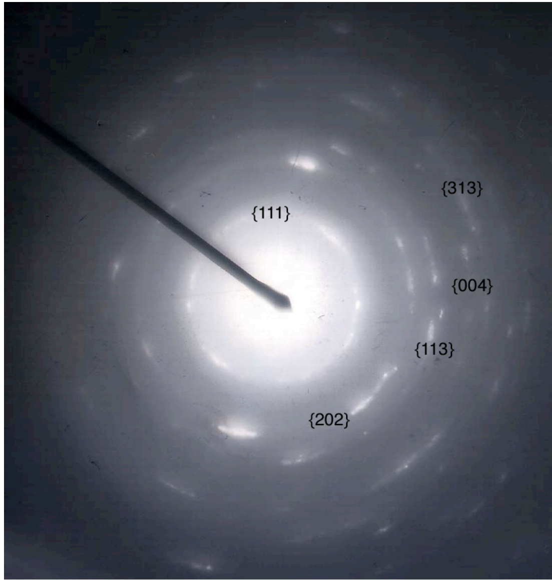

Fig. 4: Electron diffraction pattern obtained after transfer of nanocrystals to another surface. The powder diffraction rings indicate the presence of randomly oriented Ge nanocrystals on the surface.

phonon modes rather than reduced crystal sizes. Therefore, the etching process does not significantly affect nanocrystal sizes and it is possible to draw direct comparisons between as-grown nanocrystals within the matrix and liberated nanocrystals.

The Ge atomic distribution measured by RBS of etched samples, as shown in Fig. 3, reveals that 74% of the implanted Ge accumulates on the surfaces after removal of the SiO_2 matrix. Any Ge not found in nanocrystalline form, including GeO_2 in the near surface region, is expected to be etched away along with the matrix. Taking into account the oxidized Ge atoms near the surface, this suggests that the great majority of available Ge is in nanocrystalline form. At the conclusion of annealing, coarsening is most likely the main growth mechanism and further annealing would lead to less homogeneous nanocrystal size distributions.

Electron diffraction patterns confirm that nanocrystals can be successfully transferred to other surfaces for further analysis without significant reduction in their crystalline qualities. While these data indicate that nanocrystals have been successfully transferred, their arrangement on the surface has not yet been determined. Since the nanocrystal surfaces are not specially passivated, agglomeration is likely. Experiments are in progress to further develop and characterize the solution transfer process.

CONCLUSION

Isotopically pure Ge nanocrystals have been successfully produced by way of selective ion implantation of ^{70}Ge or ^{74}Ge into SiO_2 followed by thermal annealing. Raman spectra of as-grown samples exhibit asymmetric line broadening consistent with phonon confinement. However, blueshifted Raman peaks indicate that the as-grown nanocrystals are under high levels of compressive stress. Liberation of the nanocrystals from the matrix is achieved via selective HF vapor etching of the SiO_2. Raman spectra before and after etching indicate that no significant reduction of nanocrystal size occurs as a result of attack by the HF etchant. Moreover, the stress, which is present in the as-grown nanocrystals, is alleviated by removal of the oxide matrix. Liberated Ge nanocrystals are found to be stable in ambient atmospheric conditions through the longest duration experiments, which lasted five months. However, the reduction of low energy surface phonon modes over time suggests the formation of a few monolayers of oxide on the

surfaces of exposed nanocrystals. Nanocrystals can be removed from surfaces of etched samples by ultrasonic agitation (cleaning) in methanol and transferred to other surfaces from solution without loss of crystallinity. Additionally, it is likely that this liberation and transfer process, which has been specifically designed for Ge nanocrystals, may be suitable for use with other nanocrystalline materials systems. In particular, Si nanocrystals possess the same resistance to HF etching as Ge, although the rate of native oxide formation is greater in Si.

Accurate control of nanocrystal stress states, along with control of crystal size, may be used for precise band gap engineering of nanocrystals. Successful development of processes to liberate and transfer nanocrystals formed via ion implantation greatly expands the range of tools available for characterization of surface, electrical, and mechanical properties of nanocrystals. Furthermore, it enables direct manipulation of these nanocrystals for the formation of physically interesting and useful structures and arrays to explore the properties of both interacting and isolated nanocrystal systems.

ACKNOWLEGMENTS

This work was supported in part by US NSF Grant No. DMR-0109844, and by the Director, Office of Science, Office of Basic Energy Sciences, Division of Materials Sciences and Engineering, of the U.S. Department of Energy under Contract No. DE-AC03-76SF00098.

REFERENCES

1. L. Rebohle, J. von Borany, H. Fröb, and W. Skorupa, Appl. Phys. B **71**, 131 (2000).
2. H.I. Hanafi, S. Tieari, and I. Khan, IEEE Trans. Electron Devices **43**, 1553 (1996).
3. T. Takagahara and K. Takeda, Phys. Rev. B **46**, 15 578 (1992).
4. M. Yamamoto, T. Kashikawa, T. Yasue, H. Harima, and K. Kajiyama, Thin Solid Films **369**, 100 (2000).
5. W. Skorupa, L. Rebohle, and T. Gebel, Appl. Phys. A **76**, 1049 (2003).
6. M. Fujii, S. Hayashi, and K. Yamamoto, Jpn. J. Appl. Phys. **30**, 687 (1991).
7. Y. Maeda, N. Tsukamoto, Y. Yazawa, Y. Kanemitsu, and Y. Matsumoto, Appl. Phys. Lett. **59**, 3168 (1991).
8. J.P. Wilcoxon, P.P. Provencio, and G.A. Samara, Phys. Rev. B **64**, 035417 (2001).
9. E.E. Haller, J. Appl. Phys. **77**, 2857 (1995).
10. K.H. Heinig, B. Schmidt, A. Markwitz, R. Grötzschel, M. Strobel, and S. Oswald, Nucl. Instrum. Methods B **142**, 969 (1999).
11. S. Oswald, B. Schmidt, and K.H. Heinig, Surf. Interface Anal. **29**, 249 (2000).
12. H. Richter, Z.P. Wang, and L. Ley, Solid State Commun. **39**, 625 (1981).
13. F. Cerdeira, C.J. Buchenauer, F.H. Pollak, and M. Cardona, Phys. Rev. B **5**, 580 (1971).